

QUANTUM COMPUTING

Defining and detecting quantum speedup

Troels F. Rønnow,¹ Zhihui Wang,^{2,3} Joshua Job,^{3,4} Sergio Boixo,^{5,6} Sergei V. Isakov,⁷ David Wecker,⁸ John M. Martinis,⁹ Daniel A. Lidar,^{2,3,4,6,10} Matthias Troyer^{1*}

The development of small-scale quantum devices raises the question of how to fairly assess and detect quantum speedup. Here, we show how to define and measure quantum speedup and how to avoid pitfalls that might mask or fake such a speedup. We illustrate our discussion with data from tests run on a D-Wave Two device with up to 503 qubits. By using random spin glass instances as a benchmark, we found no evidence of quantum speedup when the entire data set is considered and obtained inconclusive results when comparing subsets of instances on an instance-by-instance basis. Our results do not rule out the possibility of speedup for other classes of problems and illustrate the subtle nature of the quantum speedup question.

The interest in quantum computing originates in the potential of a quantum computer to solve certain computational problems much faster than is possible classically. Examples are the factoring of integers (1) and the simulation of quantum systems (2, 3). In these examples, a quantum algorithm is exponentially faster than the best known classical algorithm. According to the extended Church-Turing thesis, all classical computers are equivalent up to polynomial factors (4). Similarly, all proposed models of quantum computation are polynomially equivalent, so that a finding of exponential quantum speedup will be model-independent. In other cases, in particular on small devices or when the quantum speedup is polynomial, defining and detecting quantum speedup becomes more subtle.

Denoting the time used by a specific classical device or algorithm to solve a problem of size N

by $C(N)$ and the time used on the quantum device by $Q(N)$, we define quantum speedup as the asymptotic behavior of the ratio

$$S(N) = \frac{C(N)}{Q(N)} \quad (1)$$

for $N \rightarrow \infty$. Subtleties appear in the choice of classical algorithms and in defining $C(N)$ and $Q(N)$ if the runtime depends not just on the size N of a problem but also on the specific problem instance and in extrapolating to the asymptotic limit.

Depending on our knowledge of classical algorithms for a given problem, we may consider four different types of quantum speedup. The optimal scenario is one of a provable quantum speedup, where there exists a proof that no classical algorithm can outperform a given quantum

algorithm. The best known example is Grover's search algorithm (5), which, in the query complexity setting, exhibits a provable quadratic speedup over the best possible classical algorithm (6). A strong quantum speedup was defined in (7) by using the performance of the best classical algorithm for $C(N)$, whether such an algorithm is known or not. Unfortunately, the performance of the best classical algorithm is unknown for many interesting problems. In the case of factoring, for example, a proof of a classical super-polynomial lower bound is not known. A less ambitious goal is therefore desirable, and thus one usually defines quantum speedup (without additional adjectives) by comparing it with the best available classical algorithm instead of the best possible classical algorithm.

A weaker scenario is one where a quantum algorithm is designed to make use of quantum effects, but it is not known whether these quantum effects provide an advantage over classical algorithms or where a device is a putative or candidate quantum information processor. To capture this scenario, which is of central interest

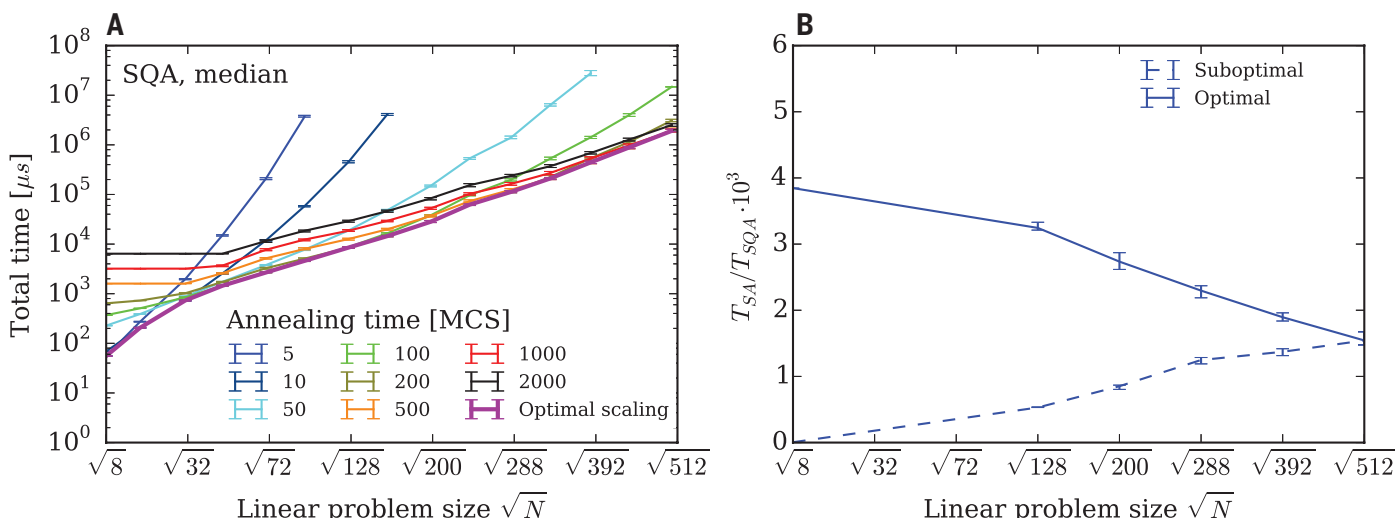


Fig. 1. Pitfalls when detecting speedup. (A) The typical (median) time to find a ground state at least once with 99% probability for spin glasses with ± 1 couplings using SQA at constant t_a . The lower envelope of the curves at constant t_a corresponds to the total effort at $t_a^{\text{opt}}(N)$ and can be used to infer the asymptotic scaling. The initial, relatively flat slope at fixed N is due to suboptimal performance at small N values and should therefore not be interpreted as speedup. Annealing

times are given in units of Monte Carlo steps (MCS), corresponding to one update per spin. (B) The speedup of SQA over SA for two cases. If SQA is run suboptimally at small sizes by choosing a fixed large $t_a = 10,000$ MCS (dashed line), a speedup is feigned. This is due to suboptimal performance on small sizes and not indicative of the real asymptotic behavior when both codes are run optimally (solid line). Error bars indicate statistical errors.

to us in this work, we define limited quantum speedup as a speedup obtained when compared specifically with classical algorithms that “correspond” to the quantum algorithm in the sense that they implement the same algorithmic approach, but on classical hardware. A natural example is quantum annealing (8, 9) or adiabatic quantum optimization (10) implemented on a candidate physical quantum information processor versus corresponding classical algorithms such as simulated annealing (SA) (11) (which performs annealing on a classical Monte Carlo simulation of the Ising spin glass and makes no use of quantum effects) or simulated quantum annealing (SQA) (12, 13) (a classical algorithm mimicking quantum annealing in a path-integral quantum Monte Carlo simulation). In this comparison, a limited quantum speedup would be a demonstration that quantum effects improve the annealing algorithm.

To illustrate the subtleties in detecting quantum speedup, even after a classical reference algorithm is chosen, we compared the performance of an experimental 503-qubit D-Wave Two (DW2, D-Wave Systems, Incorporated, Burnaby, Canada) device to classical algorithms and analyzed the evidence for quantum speedup on the benchmark problem of random spin glass instances. Specifically, we considered the problem of finding the ground state of an Ising spin glass model described by a “problem Hamiltonian”

$$H_{\text{Ising}} = -\sum_{i \in \mathcal{V}} h_i \sigma_i^z - \sum_{(i,j) \in \mathcal{E}} J_{ij} \sigma_i^z \sigma_j^z \quad (2)$$

with N binary variables $\sigma_i^z = \pm 1$. The local fields $\{h_i\}$ and couplings $\{J_{ij}\}$ are fixed and define a problem instance of the Ising model. The spins occupy the vertices \mathcal{V} of a graph $G = \{\mathcal{V}, \mathcal{E}\}$ with edge set \mathcal{E} . We will consider the distributions of the time to solution over many random spin glass problems instances with zero local fields on the Chimera graph realized by the DW2 device [see supplementary materials (14) for a definition

of that graph and why we choose $h_i = 0$]. This problem is NP-hard (15), and all known classical algorithms scale super-polynomially not only for the hardest but also for typical instances. Although quantum mechanics is not expected to reduce the super-polynomial scaling to polynomial, a quantum algorithm might still scale better with problem size N than any classical algorithm.

The D-Wave devices (16–19) are designed to be physical realizations of quantum annealing using superconducting flux qubits and programmable fields $\{h_i\}$ and couplings $\{J_{ij}\}$. Quantum annealing is implemented by initializing the system in the ground state of a transverse magnetic field $H_X = -\sum_{i \in \mathcal{V}} \sigma_i^x$, where the σ 's denote the Pauli matrices; H_X is turned off adiabatically, while H_{Ising} is turned on simultaneously. A measurement of each qubit in the computational basis then determines the ground state of H_{Ising} with a probability affected by many factors, including thermal excitations and implementation errors (20). Tests on D-Wave One (DW1) (21) and DW2 devices (22) have shown that for small problem sizes the device correlates well with the predictions of a quantum master equation. For larger problem sizes, a 108-qubit DW1 device correlated well with SQA (20), which indicates that, despite decoherence and coupling to a thermal bath, the behavior of the device is consistent with it actually performing quantum annealing (23, 24). However, for these benchmarks both SQA and the DW1 device are also well described by a semi-classical mean-field version of SQA (25), which raises the question of whether quantum effects play an important role. The approach adopted here, of seeking evidence of a (limited) quantum speedup, directly addresses the crucial question of whether large-scale quantum effects create a potential for the devices to outperform classical algorithms. To test this possibility, we compared the performance of a DW2 device to two “corresponding” classical algorithms: SA and SQA.

Because quantum speedup concerns the asymptotic scaling of $S(N)$, we considered the

subtleties of estimating it from small N and inefficiencies at small N that can fake or mask a speedup. In the context of annealing, the optimal choice of the annealing time t_a turns out to be crucial for estimating asymptotic scaling. To illustrate this, we first considered the time to solution using SA and SQA run at different fixed t_a values, independent of N . Figure 1A shows the scaling of the median total annealing time [over 1000 different random instances on the D-Wave Chimera graph; see supplementary materials (14)] for SQA to find a solution at least once with probability $P = 0.99$. Corresponding times for SA are shown in fig. S10. We observed that at constant t_a , as long as t_a is long enough to find the ground state almost every time, the scaling of the total effort is at first relatively flat. The total effort then rose more rapidly, once one reached N values for which the chosen t_a is too short, and the success probabilities were thus low, requiring many repetitions. Extrapolations to $N \rightarrow \infty$ need to consider the lower envelope of all curves, which corresponds to choosing an optimal annealing time $t_a^{\text{opt}}(N)$ for each N .

Figure 1B demonstrates that, when using fixed t_a values, no conclusion can be drawn from annealing (simulated or in a device) about the asymptotic scaling. The initial slow increase at constant t_a is misleading, and instead the optimal annealing time t_a^{opt} needs to be used for each N . To illustrate this, we show (Fig. 1B) the real “speedup” ratio of the scaling of SA and SQA (actually a slowdown) and a fake speedup resulting from a constant and excessively long t_a for SQA. Because SA outperforms SQA on our benchmark set, it is our algorithm of choice in the comparisons with the DW2 reported below.

A related issue is the scaling of hardware resources (computational gates and memory) with problem size, which must be identical for the devices we compare. A device whose hardware resources scale as N can achieve an intrinsic parallel speedup compared with a fixed

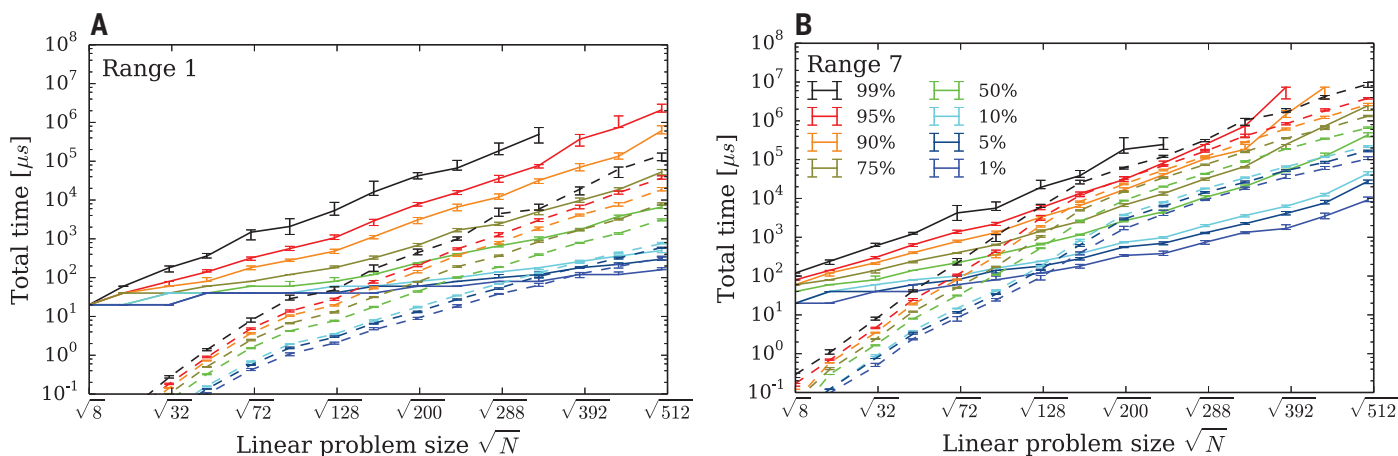


Fig. 2. Scaling of time to solution for $r = 1$ (A) and $r = 7$ (B). Shown is the scaling of the pure annealing time to find the ground state at least once with a probability $P = 0.99$ for various quantiles of hardness for simulated annealing (SA, dashed) and the DW2 (solid). The solid lines terminate for the highest quantiles because the DW2 did not solve the hardest instances for large problem sizes within the maximum number of repetitions (at least 32,000) of the annealing we performed.

size device. Such is the case for the DW2, which uses N (out of 512) qubits, $\mathcal{O}(N)$ couplers, and $\mathcal{O}(N)$ classical logical control gates to solve a spin glass instance with N spin variables in time $T_{\text{DW}}(N)$. Considering quantum speedup for $N \rightarrow \infty$, we need to compare a (hypothetical) larger DW2 device with the number of qubits and couplers growing as $\mathcal{O}(N)$ to a (hypothetical) classical device with $\mathcal{O}(N)$ gates or processing units. Because SA (and SQA) are perfectly parallelizable for the bipartite Chimera graphs realized by the DW2, we can relate the scaling of the time $T_{\text{C}}(N)$ on such a device to the time $T_{\text{SA}}(N)$ for SA on a fixed-size classical central processing unit (CPU) by $T_{\text{C}}(N) \sim T_{\text{SA}}/N$ and obtain

$$S(N) = \frac{T_{\text{C}}(N)}{T_{\text{DW}}(N)} \sim \frac{T_{\text{SA}}(N)}{T_{\text{DW}}(N)} \frac{1}{N} \quad (3)$$

We lastly addressed the question of how to measure time when the time to solution depends on the specific problem instance. When a device

is used as a tool for solving computational problems, the question of interest is to determine which device is better for almost all possible problem instances. If instead the focus is on the underlying physics of a device, then it might suffice to find a subclass of instances where a speedup is exhibited. These two questions lead to different quantities of interest.

To illustrate the considerations, we now turn to our results. Figure 2 shows the scaling of the time to find the ground state for various quantiles, from the easiest instances (1%) to the hardest (99%), comparing the DW2 and SA. We chose the values of the couplings J_{ij} from $2r$ discrete values $\{n/r\}$, with $n \in \{\pm 1, \dots, r-1, r\}$, and call r the range. Because we do not a priori know the hardness of a given problem instance, we have to assume the worst case and perform a sufficient number of repetitions R to be able to solve even the hardest problem instances. Hence, the scaling for the highest quantiles is the most informative. Here, we considered only the pure annealing times, ignoring setup and

readout times that scale subdominantly [see (14) for wall-clock results].

We observed for both the DW2 and the SA, for sufficiently large N , that the total time to solution for each quantile q scaled as $\exp(c_q \sqrt{N})$ (with $c_q > 0$ a constant) as reported previously for SA and SQA (20). The origin of the \sqrt{N} exponent is well understood for exact solvers as reflecting the treewidth of the Chimera graph (14, 26). Whereas the SA code was run at a t_a^{opt} for each N , the DW2 has a minimal $t_a = 20 \mu\text{s}$, which is longer than the optimal time for all problem sizes (14). Therefore, the observed slope of the DW2 data can only be taken as a lower bound for the asymptotic scaling. With this in mind, we observed similar scaling for SA and the DW2 for $N \geq 200$.

How can we probe for a speedup in light of this similar scaling? With algorithms such as SA or quantum annealing, where the time to solution depends on the problem instance, it is impractical to experimentally find the hardest problem instance. If instead we target a fraction

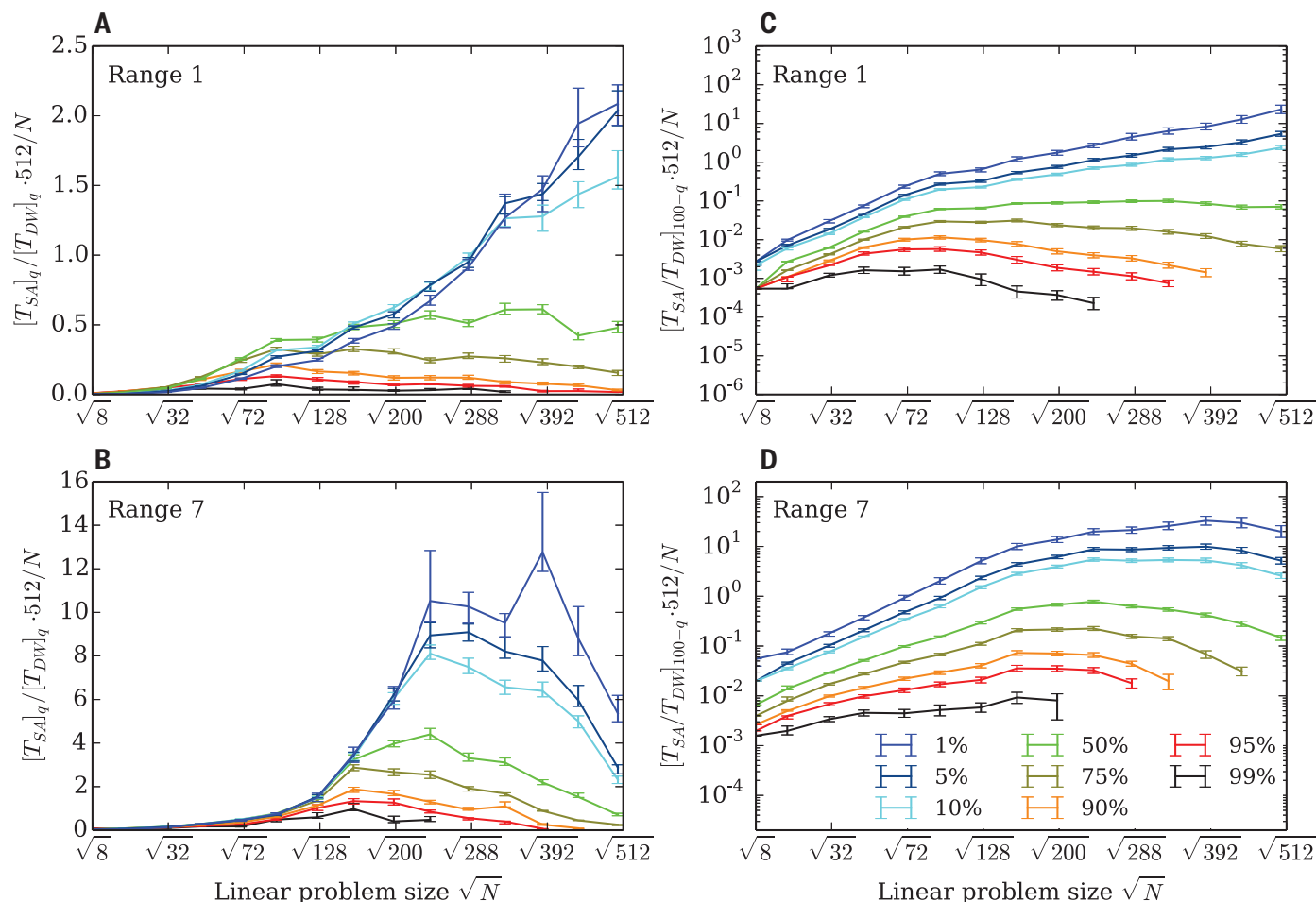


Fig. 3. Speedup of the DW2 compared to SA. (A and B) For the RofQs, and (C and D) for the QofRs. For a random variable X with distribution $p(x)$ and values in $x \in [0, \infty)$, we defined, as usual, the q th quantile as $\int_0^q p(x)dx = q/100$, which we solved for x_q and plotted as a function of \sqrt{N} . In the QofR case, we used x_{100-q} so that high quantiles still corresponded to instances that are hard for the DW2. We terminated the curves when the DW2 does

not find the ground state for large N at high percentiles. In these plots, we multiplied Eqs. 4 and 5 by 512 so that the speedup value at $N = 512$ directly compares one DW2 processor against one classical CPU. An overall positive slope suggests a possible limited quantum speedup, subject to the caveats discussed in the text. A negative slope indicates that SA outperforms the DW2.

of $q\%$ of the instances, then we should consider the q th quantile in the scaling plots shown in Fig. 2. The appropriate speedup quantity is then the ratio of these quantiles (RofQ). Denoting a quantile q of a random variable X by $[X]_q$, we define this as

$$S_q^{\text{RofQ}}(N) = \frac{[T_{\text{SA}}(N)]_q}{[T_{\text{DW}}(N)]_q} \frac{1}{N} \quad (4)$$

Plotting this quantity for the DW2 versus SA in Fig. 3, A and B, we found no evidence for a limited quantum speedup in the interesting regime of large N and large q (almost all instances). That is, although for all quantiles and for both ranges the initial slope was positive, when N and q became large enough we observed a turnaround and eventually a negative slope. Although we observed a positive slope for quantiles smaller than the median, this is of limited interest because we have not been able to identify a priori which instances will be easy. Taking into account that because of the fixed suboptimal annealing times the speedup defined in Eq. 4 is an upper bound, we conclude that there is no evidence of a speedup over SA for this particular benchmark.

$S_q^{\text{QofR}}(N)$ measures the speedup while comparing different sets of instances for DW and SA, each determined by the respective quantile. Now we consider instead whether there is a speedup for a (potentially small) subset of the same problem instances. To this end, we study the scaling of the ratios of the time to solution for individual instances and display in Fig. 3, C and D, the scaling of various quantiles of the ratio (QofR)

$$S_q^{\text{QofR}}(N) = \left[\frac{T_{\text{SA}}(N)}{T_{\text{DW}}(N)} \right]_q \frac{1}{N} \quad (5)$$

For $r = 7$, all the quantiles bend down for sufficiently large N , so that there is no evidence of a

limited quantum speedup. There does seem to be an indication of such a speedup compared to SA in the low quantiles for $r = 1$, that is, for those instances whose speedup ratio was high. However, the instances contributing here are not run at t_a^{opt} , and more work is needed to establish that the potential $r = 1$ speedup result persists for those instances for which one can be sure that t_a is optimal.

Next we consider the distribution of solution times at a fixed problem size. This does not address the speedup question, because no scaling can be extracted, but illuminates instead the question of correlation between the performance of the DW2 and SA. To this end, we performed individual comparisons for each instance and show in Fig. 4, A and B, the time to solution for the same instances for the DW2 and SA. We observed a wide scatter [in agreement with the DW1 results of (20)] and found that, although the DW2 is sometimes up to 10 times faster in pure annealing time, there are many cases where it is ≥ 100 times slower.

It is not yet known whether a quantum annealer or even a perfectly coherent adiabatic quantum optimizer can exhibit (limited) quantum speedup at all, although there are promising indications from theory (27), simulation (13), and experiments on spin glass materials (9). Experimental tests are thus important. There are several candidate explanations for the absence of a clear quantum speedup in our tests. Perhaps quantum annealing simply does not provide any advantages over simulated (quantum) annealing or other classical algorithms for the problem class we have studied (28), or perhaps the noisy implementation in the DW2 cannot realize quantum speedup and is thus not better than classical devices. Alternatively, a speedup might be masked by calibration errors, improvements might arise from error correction (29), or other problem classes might exhibit a speedup. Future studies will probe

these alternatives and aim to determine whether one can find a class of problem instances for which an unambiguous speedup over classical hardware can be observed.

Although we used specific processors and algorithms for illustration, the considerations about a reliable determination of quantum speedup presented here are general. For any speedup analysis, use of the same scaling of hardware resources for both quantum and classical devices is required to disentangle parallel and quantum speedup. And, for any quantum algorithm where the runtime must be determined experimentally, a careful extrapolation to large problem sizes is important to avoid mistaking inefficiencies at small problem sizes for signs of quantum speedup.

REFERENCES AND NOTES

- P. W. Shor, in *Proceedings 35th Annual Symposium on Foundations of Computer Science* (IEEE, New York, 1994), pp. 124–134.
- R. Feynman, *Int. J. Theor. Phys.* **21**, 467–488 (1982).
- S. Lloyd, *Science* **273**, 1073–1078 (1996).
- I. Parberry, *SIGACT News* **18**, 54–67 (1986).
- L. K. Grover, *Phys. Rev. Lett.* **79**, 325–328 (1997).
- C. Bennett, E. Bernstein, G. Brassard, U. Vazirani, *SIAM J. Comput.* **26**, 1510–1523 (1997).
- A. Papageorgiou, J. F. Traub, *Phys. Rev. A* **88**, 022316 (2013).
- T. Kadowaki, H. Nishimori, *Phys. Rev. E* **58**, 5355–5363 (1998).
- J. Brooke, D. Bitko, T. F. Rosenbaum, G. Aeppli, *Science* **284**, 779–781 (1999).
- E. Farhi et al., *Science* **292**, 472–475 (2001).
- S. Kirkpatrick, C. D. Gelatt Jr., M. P. Vecchi, *Science* **220**, 671–680 (1983).
- R. Martoňák, G. E. Santoro, E. Tosatti, *Phys. Rev. B* **66**, 094203 (2002).
- G. E. Santoro, R. Martoňák, E. Tosatti, R. Car, *Science* **295**, 2427–2430 (2002).
- See supplementary materials on Science Online. The supplementary materials provide details about the classical simulation algorithms, the DW2 device, the procedure used to determine annealing times, and additional data on scaling with problem size.
- F. Barahona, *J. Phys. Math. Gen.* **15**, 3241–3253 (1982).
- R. Harris et al., *Phys. Rev. B* **82**, 024511 (2010).
- M. W. Johnson et al., *Supercond. Sci. Technol.* **23**, 065004 (2010).
- A. J. Berkley et al., *Supercond. Sci. Technol.* **23**, 105014 (2010).
- M. W. Johnson et al., *Nature* **473**, 194–198 (2011).
- S. Boixo et al., *Nat. Phys.* **10**, 218–224 (2014).
- S. Boixo, T. Albash, F. M. Spedalieri, N. Chancellor, D. A. Lidar, <http://arxiv.org/abs/1212.1739> (2012).
- W. Vinci, T. Albash, A. Mishra, P. A. Warburton, D. A. Lidar, <http://arxiv.org/abs/1403.4228> (2014).
- J. A. Smolin, G. Smith, <http://arxiv.org/abs/1305.4904> (2013).
- L. Wang et al., <http://arxiv.org/abs/1305.5837> (2013).
- S. W. Shin, G. Smith, J. A. Smolin, U. Vazirani, <http://arxiv.org/abs/1401.7087> (2014).
- V. Choi, *Quantum Inf. Process.* **10**, 343–353 (2011).
- R. D. Somma, D. Nagaj, M. Kieferová, *Phys. Rev. Lett.* **109**, 050501 (2012).
- H. G. Katzgraber, F. Hamze, R. S. Andrist, *Phys. Rev. X* **4**, 021008 (2014).
- K. L. Pudenz, T. Albash, D. A. Lidar, *Nat. Commun.* **5**, 3243 (2014).
- S. Isakov, I. Zintchenko, T. Rønnow, M. Troyer, <http://arxiv.org/abs/1401.1084> (2014).

ACKNOWLEDGMENTS

We thank N. Allen, M. Amin, E. Farhi, M. Mohseni, H. Neven, and C. McGeoch for useful discussions and comments and I. Zintchenko for providing the an_ss_ge_nf_bp simulated annealing code before publication of the code with (30). This project was supported by the Swiss National Science Foundation through the

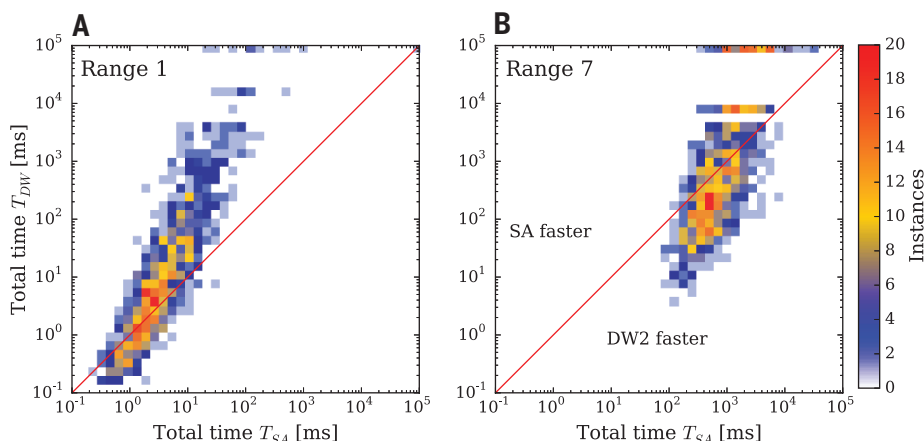


Fig. 4. Instance-by-instance comparison of annealing times. Shown are scatter plots of the pure annealing time for the DW2 compared with SA using an average over 16 gauges [see (14)] on the DW2 for (A) $r = 1$ and (B) $r = 7$. The color scale indicates the number of instances in each square. Instances below the diagonal red line are faster on the DW2; those above are faster using SA. Instances for which the DW2 did not find the solution with 10,000 repetitions per gauge are shown at the top of the frame (no such instances were found for SA).

National Center of Competence in Research Quantum Science and Technology, the Army Research Office (ARO) Multidisciplinary University Research Initiative (MURI) grant no. W911NF11-1-0268, ARO grant no. W911NF-12-1-0523, the Lockheed Martin Corporation, and Microsoft Research. Simulations were performed on clusters at Microsoft Research and ETH Zurich on supercomputers of the Swiss Center for Scientific Computing.

We acknowledge hospitality of the Aspen Center for Physics, supported by NSF grant PHY-1066293.

SUPPLEMENTARY MATERIALS

www.sciencemag.org/content/345/6195/420/DC1
Supplementary Text
Figs. S1 to S10

Tables S1 and S2
References (31–37)

17 February 2014; accepted 10 June 2014
Published online 19 June 2014;
10.1126/science.1252319

QUANTUM METROLOGY

Fisher information and entanglement of non-Gaussian spin states

Helmut Strobel,^{1*} Wolfgang Muessel,¹ Daniel Linnemann,¹ Tilman Zibold,¹ David B. Hume,¹ Luca Pezzè,² Augusto Smerzi,² Markus K. Oberthaler¹

Entanglement is the key quantum resource for improving measurement sensitivity beyond classical limits. However, the production of entanglement in mesoscopic atomic systems has been limited to squeezed states, described by Gaussian statistics. Here, we report on the creation and characterization of non-Gaussian many-body entangled states. We develop a general method to extract the Fisher information, which reveals that the quantum dynamics of a classically unstable system creates quantum states that are not spin squeezed but nevertheless entangled. The extracted Fisher information quantifies metrologically useful entanglement, which we confirm by Bayesian phase estimation with sub-shot-noise sensitivity. These methods are scalable to large particle numbers and applicable directly to other quantum systems.

Multiparticle entangled states are the key ingredients for advanced quantum technologies (1). Various types have been achieved in experimental settings ranging from ion traps (2), photonic systems (3), and solid state circuits (4) to Bose-Einstein condensates. For the latter, squeezed states (5, 6) have been generated (7–12), and a rich class of entangled non-Gaussian states is predicted to be obtainable (13), including maximally entangled Schrödinger cat states (14, 15). The production of these fragile states in large systems remains a challenge, and efficient methods for characterization are necessary because full state reconstruction becomes intractable. Here, we generate a class of non-Gaussian many-particle entangled states and reveal their quantum properties by studying the distinguishability of experimental probability distributions.

A measure of the distinguishability with respect to small phase changes of the state is provided by the Fisher information F (16). It is related to the highest attainable interferometric phase sensitivity by the Cramer-Rao bound $\Delta\theta_{\text{CR}} = 1/\sqrt{F}$ (17). This limit follows from general statistical arguments for a measurement device with fluctuating output (18). The Fisher information is limited by quantum fluctuations of the input state as

well as the performance of the device. Even in the absence of technical noise, the Fisher information of a classical input state is $F \leq N$ because

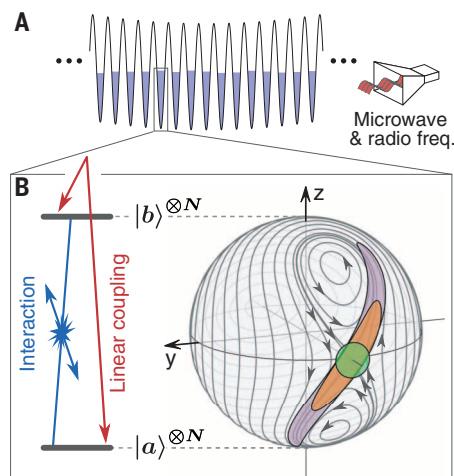


Fig. 1. Preparation and detection of non-Gaussian entangled states. (A) Array of Bose-Einstein condensates in an optical lattice potential addressed by microwave and radio frequency fields. (B) The interplay of nonlinear interaction (blue) and weak Rabi coupling (red) between the internal states $|a\rangle$ and $|b\rangle$ results in an unstable fixed point in the classical phase space. The state of the system is visualized on a generalized Bloch sphere with radius $J = N/2$. Gray lines indicate trajectories of the mean-field equations of motion (18). The initial coherent spin state (green) ideally evolves into a squeezed state (orange) followed by non-Gaussian states at later evolution times (violet). Edges of shaded areas are contours of the Husimi distribution for $N = 380$ at $1/e^2$ of its maximum. (C) Experimental absorption picture showing the site- and state-resolved optical lattice after a Stern-Gerlach separation. Shaded boxes indicate the sites with a total atom number in the range of 380 ± 15 , which are selected for further analysis. (D) Example histograms of the imbalance $z = 2J_z/N$ after nonlinear evolution of 25 ms and final rotation (angles indicated in the graphs) compared with the ideal coherent spin state of identical N (green Gaussian).

¹Kirchhoff-Institut für Physik, Universität Heidelberg, Im Neuenheimer Feld 227, 69120 Heidelberg, Germany. ²QSTAR (Quantum Science and Technology in Arcetri), INO-CNR (Istituto Nazionale di Ottica–Consiglio Nazionale delle Ricerche), and LENS (European Laboratory for Nonlinear Spectroscopy), Largo Enrico Fermi 2, 50125 Firenze, Italy.
*Corresponding author. E-mail: fisherinformation@matterwave.de

Defining and detecting quantum speedup

Troels F. Rønnow, Zhihui Wang, Joshua Job, Sergio Boixo, Sergei V. Isakov, David Wecker, John M. Martinis, Daniel A. Lidar and Matthias Troyer

Science **345** (6195), 420-424.
DOI: 10.1126/science.1252319 originally published online June 19, 2014

How to benchmark a quantum computer

Quantum machines offer the possibility of performing certain computations much faster than their classical counterparts. However, how to define and measure quantum speedup is a topic of debate. Rønnow *et al.* describe methods for fairly evaluating the difference in computational power between classical and quantum processors. They define various types of quantum speedup and consider quantum processors that are designed to solve a specific class of problems.

Science, this issue p. 420

ARTICLE TOOLS

<http://science.sciencemag.org/content/345/6195/420>

SUPPLEMENTARY MATERIALS

<http://science.sciencemag.org/content/suppl/2014/06/18/science.1252319.DC1>

RELATED CONTENT

<http://science.sciencemag.org/content/sci/344/6190/1330.full>

REFERENCES

This article cites 27 articles, 5 of which you can access for free
<http://science.sciencemag.org/content/345/6195/420#BIBL>

PERMISSIONS

<http://www.sciencemag.org/help/reprints-and-permissions>

Use of this article is subject to the [Terms of Service](#)